Materials Science and Engineering, 43 (1980) 151 - 158

On the Dissolution Kinetics of Silicon in an Aluminium-rich Matrix

S. K. PABI

Materials Science Centre, Indian Institute of Technology, Kharagpur, West Bengal 721302 (India)

(Received May 19, 1979; in revised form September 10, 1979)

SUMMARY

Large silicon precipitates preformed in Al–0.57at.%Si alloy by a special thermal treatment were partially dissolved in the matrix by up-quenching, and the evolution with time of concentration fields adjacent to several precipitates was measured using quantitative microprobe analyses. A computer analysis of the data through non-linear regression yielded the solute content of the matrix at the phase boundaries and the diffusion coefficient of silicon in the dilute Al–Si alloy. An examination of these parameters revealed that an interface reaction controls the dissolution process and that the solution kinetics can vary from one particle to another possibly because of the variation in the structure of the phase boundaries. Some differences were observed in solute transfer characteristics across the low energy and high energy precipitate–matrix interfaces. However, the present diffusion data agree reasonably with information available in the literature.

1. INTRODUCTION

The aluminium metallization layer in silicon devices frequently interacts with the wafer [1]. Naturally the kinetics of the precipitation and dissolution of silicon into the evaporated aluminium layers have received wide attention in recent years [2 - 6]. Contamination of the interface can exert a marked influence on the diffusive transfer of silicon [7 - 9]. However, if the silicon wafer is cleared of surface impurities prior to metallization the dissolution of silicon into the evaporated aluminium layer takes place in such a manner that the Si–Al interface assumes a simple shape composed of a few {111} Si facets [6]. Clearly crystal planes other than {111} Si dissolve more rapidly and hence grow out. From this observation it may be anticipated that the dissolution of silicon in aluminium is an interface-controlled process.

To obtain an insight into the dissolution process we undertook an investigation on wrought Al–0.57%Si* alloy. Below the solvus temperature almost pure elemental silicon precipitates out in this alloy [10, 11]. The second phase can occur as both plate-like and equiaxed particles [12, 13]. The plates are often triangular or hexagonal. A careful X-ray study [13] of single-crystal Al–1%Si alloy water quenched from the homogenization temperature has revealed certain preferred crystallographic orientations of the precipitated particles. The orientation preference diminishes with over-aging and is not found at all when specimens are air cooled instead of water quenched. Nevertheless, contamination of the silicon–matrix interface is not likely to be significant in a bulk sample prepared from high purity ingredients. Therefore for homogenization studies these precipitates may be partially dissolved by up-quenching.

In studying the kinetics of a diffusional transformation an indirect approach can often be misleading, as has been demonstrated by Hillert [14], and a direct measurement of the compositions at the interface will yield more reliable results. In the present work we proposed to measure the evolution with time of concentration fields adjacent to dissolving precipitates. Analyses of the data obtained give the solute concentration C_S in the matrix at the precipitate–matrix interface and the diffusivity D of silicon in the aluminium-rich matrix. These data may promote a better understanding of the dissolution process.

*Compositions are expressed in atomic per cent unless otherwise stated.

2. EXPERIMENTAL

2.1. Preparation of the specimens

The Al–Si alloy was prepared by induction melting 99.99% pure aluminium and silicon in a pure graphite crucible. Chill-cast ingots of the alloy 30 mm in diameter were homogenized at 770 K for 2 d, were hot forged at 750 K to 15 mm × 15 mm squares and finally were hot rolled to sheets 1.5 mm thick. Strips 60 mm × 20 mm in size were cut from these sheets and were heated in a tube furnace at 840 K for 7 d. This long annealing produces a thoroughly homogeneous material with a stable grain structure. The strips were subsequently furnace cooled to 770 K in 24 h, the last temperature being about 30 K above the solvus temperature for the alloy [10, 11]. Next the sample temperature was reduced very slowly to 660 K at a rate of 5 K d^{-1} and was arrested at 660 K for 10 d. Finally the strips were cooled to room temperature in an air blast. Large grain boundary allotriomorphs (see Fig. 1) up to 200 μm in length were developed using this thermal schedule. The intragranular (matrix) precipitates were usually smaller although a few of them were 30 - 100 μm long. Microprobe analyses confirmed that protracted equilibration at 660 K completely removes any composition gradient in the matrix surrounding the precipitates.

Silicon deforms very little below 900 K and fracture due to applied stress often takes place at the boundary between the aluminium and the larger silicon particles [11]. Special care was therefore taken to avoid any deformation of the samples during subsequent handling. Specimens 8 mm × 8 mm × 1.5 mm in size were cut from the rolled strips by electrospark machining and were polished with 0.5 μm diamond. Ash-coloured silicon precipitates were visible on the polished surface. The samples were etched in an aqueous solution of 0.5 vol.% HF to reveal the grain boundaries.

2.2. Selection of precipitates and dissolution studies

Several large allotriomorphs and intragranular plates with precipitate-free zones extending to about 100 μm around them were selected and identified by microhardness indentations in their vicinity. The locations of these particles with respect to grain boundaries were recorded. The etch on the specimen surface was then removed by a light diamond polish. The samples were wrapped in aluminium foil to prevent contamination and were immersed in a salt bath to dissolve the silicon precipitates partially in the aluminium-rich matrix. The solution temperature T_D was maintained at a preset level in the range 772 - 837 K and was controlled to ±1 K. The specimens were subsequently quenched in water to room temperature.

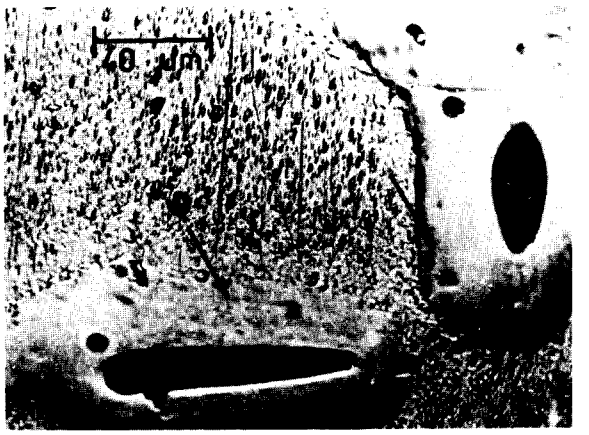

Fig. 1. The microstructure of Al–0.57%Si alloy displaying two dissolving silicon precipitates. The arrows indicate the silicon-enriched regions enveloping the precipitates and the mottled structure elsewhere is the precipitate-depleted matrix.

Figure 1 shows the solute-enriched regions around dissolving precipitates. The concentration distribution in the enriched zone across the centre of selected precipitates was measured along a line perpendicular to the trace of the precipitate using an MAR 2 electron probe microanalyser. The probe was operated at 15 kV with a beam current of 12 μA. Step scanning was carried out and the intensity of Si Kα radiation was measured. The interface position was ascertained graphically as the midpoint of the discontinuous step formed in the plot of Si Kα intensity *versus* distance when the electron beam traversed a phase boundary. The X-ray intensities were corrected for dead time, background, absorption, characteristic fluorescence, backscattering losses and ionization/penetration losses by using Colby's MAGIC IV computer program [15] and the percentages of silicon were determined. The precision of the analyses was within ±0.01% Si for the range of compositions measured. The depth of the analysed region was about 1.5 μm.

2.3. Shape and inclination of the precipitates

Approximately 10 - 15 μm of the matrix was removed by electropolishing in a bath containing 817 ml orthophosphoric acid, 134 ml sulphuric acid, 0.156 kg chromic oxide and 40 ml water using an aluminium cathode at 12 V. Because the bath was strongly oxidizing this polish was not used prior to dissolution treatments in order to avoid contamination. The silicon precipitates were not significantly attacked during this electrochemical treatment. Examination using an ISI-60 scanning electron microscope established the planar geometry of the particles selected. The angle of inclination θ was the minimum rotation of the planar surface of a precipitate required to make it vertical to the polished surface and could be determined using the tilting mechanism of the ISI-60 microscope.

3. RESULTS AND DISCUSSION

3.1. Analysis of the results

The electron probe of the microanalyser had a non-zero radius and in the vicinity of a second-phase particle a fraction of the incident electrons were scattered by the precipitate itself. As a result an apparent silicon enrichment of the aluminium-rich matrix up to a distance of about 7 μm from the interface became evident even prior to any dissolution treatment. Hence in the ensuing analyses data for regions lying within 7 μm from the phase boundary were usually ignored.

The remaining portion of the concentration–distance profiles was analysed on the basis of the following assumptions.

(i) The diffusion of aluminium in silicon concurrent with the dissolution process is negligible. This assumption appears to be well justified because extrapolation of high temperature diffusion data for aluminium in silicon [16] shows that the diffusion coefficient at 850 K is about ten orders of magnitude smaller than the diffusivity of silicon in aluminium [2, 11, 17 - 21].

(ii) The diffusion coefficient of silicon in aluminium at the dissolution temperatures is independent of concentration. Recent careful measurements by Bergner and Cyrener [21] support this view.

(iii) The position of the precipitate–matrix interface is considered to be time invariant compared with the effective penetration distance of the diffusion flux. In fact the displacement of the interface computed from the area under the concentration–distance curve is always less than 0.8 μm whereas the diffusion profiles extend to 40 - 140 μm.

(iv) The diffusion fields from neighbouring precipitates do not overlap. The time–temperature schedule was designed to attain this condition. Further, the estimated concentration distribution sometimes displayed marked discontinuities due presumably to the presence of subsurface precipitates. These profiles were discarded. From a recent analysis of dissolution in planar composites [22], however, it may be readily shown that the decay rate of the second phase remains practically unaffected by the impinging diffusion field from an adjacent particle until the trough of the interlinking concentration profile reaches about $0.4C_s + 0.6C_M$ where C_M is the solute content of the matrix prior to solution treatment.

(v) From a mathematical point of view planar surfaces of the precipitates are assumed to be infinite in extent. It should be recalled that only very large precipitates were selected for the study.

(vi) Planar faces of the precipitates are vertical to the polished surface. This criterion was strictly satisfied by only two of the selected particles and for the rest of the precipitates chosen $\theta < 0.35$ rad (20°).

For a planar source at the surface of a semi-infinite medium of uniform composition C_M the concentration–distance profile ahead of a dissolving plate can now be fitted to the equation [23]

$$C = C_M + (C_S - C_M) \operatorname{erfc} \{0.5x/(Dt)^{1/2}\} \quad (1)$$

where C is the solute content of the matrix at a distance x from the phase boundary, D is the diffusion coefficient and t is the duration of the homogenization. The correlation of the data was carried out by a curvilinear regression analysis on a computer using the "maximum neighbourhood" method of Marquardt [24]. Essentially the program attempts to optimize the values of C_S and D in order to minimize the residual δ given by

$$\delta = \sum_{i=1}^{n} (C_i - \bar{C}_i)^2 \qquad (2)$$

where n is the number of data points, C_i is the experimentally measured concentration for the ith data point and $\bar{C}_i$ is the predicted value of C for the ith data point computed from eqn. (1). The trial values of the parameters required to start the regression analysis were obtained in the following way. A smooth curve was established "by eye" through the concentration–distance data points and was extrapolated to $x = 0$ to obtain the initial estimate of C_S. This value of C_S in conjunction with a few data points and eqn. (1) leads to the starting value of D.

Figure 2 gives a typical variation of the concentration distribution with time on either side of a dissolving precipitate. Here the discrete points are the experimental data and they seem to fit closely to the lines computed from regression analysis. In fact the present regression scheme arrives at a near-optimum estimate of C_S and D in which further variation of these parameters by trial and error in order to decrease δ for any given set of experimental data shows that Marquardt's algorithm [24] produces values of C_S and D within ±2% and ±5% respectively of the estimates corresponding to a best possible fit to eqn. (1). Scans I and II reported in Fig. 2 were taken along two parallel lines 30 μm apart near the central region of the precipitate. The plots virtually coincide, showing the reproducibility of the measured profiles and the insignificance of the exact scan position in relation to the precipitate centre. A comparison of the concentration–distance curves for side 1 and side 2 (Figs. 2(a) and 2(b) respectively) shows that they are not identical, although θ for this precipitate was zero. The asymmetry becomes a little more apparent if the plate is not exactly perpendicular to the polished surface. Table 1 summarizes the results of analyses of the concentration–distance data for 16 precipitates. Here C_{SA} for any particle is the average of C_S values at a given time and temperature of dissolution. D_A is the mean diffusion coefficient.

3.2. Diffusion of silicon in the aluminium-rich matrix

Figure 3 shows a plot of log D *versus* 1000/T_D and the best straight line fit to these data. The values of D_A in Table 1 were obtained from this line. The values of D in the figure show some scatter although most of them lie within a factor of two of the estimated D_A.

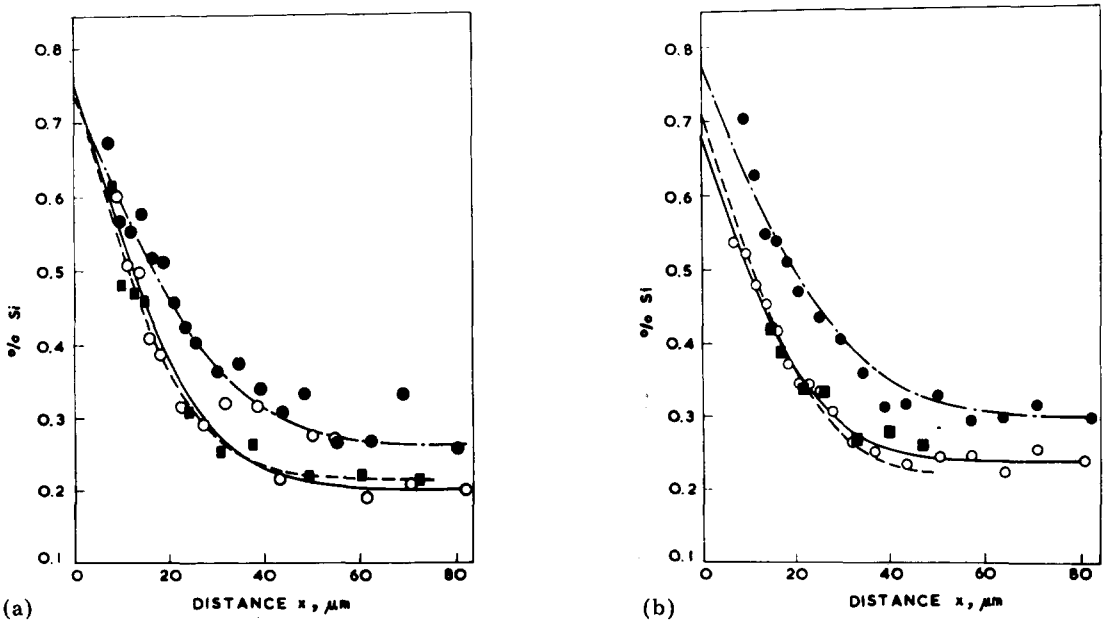

Fig. 2. The variation of the concentration distribution on both sides of a dissolving allotriomorph: precipitate 1, T_D = 772 K, θ = 0; ○, ——, 1500 s, scan I; ■, — — —, 1500 s, scan II; ●, — · —, 3000 s, scan III; (a) side 1; (b) side 2.

TABLE 1

A summary of the concentration–distance profile analyses

Precipitate	T_D (K)	*Precipitate location*	*t* (s)	*Side 1*		*Side 2*		C_{SA}	D_A
				C_S (% Si)	D ($\times 10^{-13}$ m^2 s^{-1})	C_S (% Si)	D ($\times 10^{-13}$ m^2 s^{-1})	(% Si)	($\times 10^{-13}$ m^2 s^{-1})
1	772	GB[a]	1500	0.76	1.38	0.69	1.21	0.73	1.36
				0.76	1.13	0.71	1.18		
			3000	0.75	1.04	0.77	1.04	0.76	
2	772	GB	900	0.62	1.45	0.98	4.44	0.80	1.36
			4800	0.90	1.30	1.02	1.36	0.96	
3	772	Matrix	2460	0.60	1.52	0.87	1.25	0.73	1.36
4	772	GB	2460	0.51	1.29	0.83	1.57	0.67	1.36
5	772	Matrix	2460	0.64	1.19	–	–	0.64	1.36
6	772	GB	2400	0.78	1.17	–	–	0.78	1.36
7	795	GB	480	0.79	3.30	0.89	3.06	0.84	2.76
			960	0.89	5.65	1.00	4.43	0.94	
			1920	0.85	5.31	1.31	4.58	1.08	
8	795	GB	1200	0.93	2.15	1.20	2.37	1.06	2.76
9	795	Matrix	1020	0.76	2.91	0.89	2.67	0.82	2.76
10	795	Matrix	1020	0.98	2.31	–	–	0.98	2.76
11	803	Matrix	1500	0.88	3.44	–	–	0.88	3.50
12	815	Matrix	300	–	–	0.69	4.13	0.69	4.95
			600	–	–	0.80	7.89	0.80	
			1200	–	–	1.26	4.54	1.26	
13	815	GB	600	0.79	3.87	–	–	0.79	4.95
			1200	1.11	4.44	–	–	1.11	
14	829	GB	540	1.32	5.32	1.35	5.45	1.33	7.31
15	837	GB	150	1.25	13.50	1.13	14.50	1.19	9.09
			300	1.14	11.60	1.42	13.80	1.28	
			600	1.34	7.50	1.39	7.12	1.36	
16	837	GB	150	1.11	9.37	1.66	8.17	1.38	9.09
			300	1.23	7.20	1.79	6.66	1.51	
			600	1.32	7.00	1.77	6.61	1.54	

[a]GB, grain boundary.

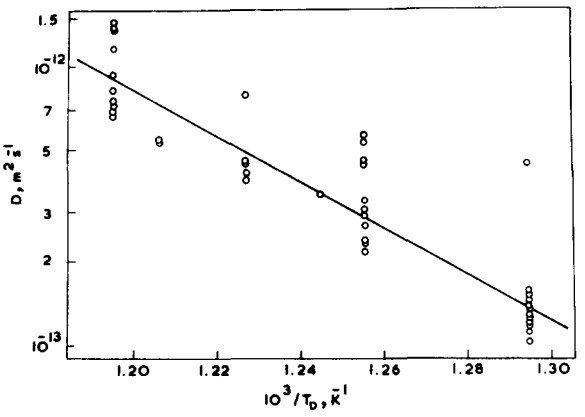

Fig. 3. An Arrhenius plot of D values obtained from the dissolution data for silicon precipitates.

The non-zero θ for several precipitates may be partly responsible for this scatter. However, the divergence appears to be typical of the Al–Si system [2, 11, 17 - 21] and Mehl *et al.* [18] have summarized the situation by giving a band of values for the diffusivity of silicon in pure aluminium, as illustrated in Fig. 4. In Fig. 4 the straight line in Fig. 3 has been superimposed on the available diffusion data for silicon in pure aluminium [2, 17 - 21]. The present results seem to be in accord with the data reported in the literature. In particular, the agreement with the recent measurements of McCaldin and Sankur [2] and Bergner and Cyrener [21] is excellent.

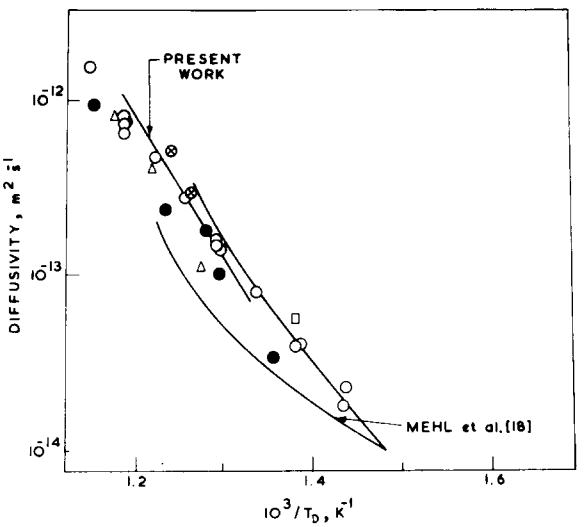

Fig. 4. A comparison of the diffusivity of silicon in wrought aluminium with the mean diffusion coefficient estimated in the present work: ⊗, from ref. 2; •, from ref. 17; △, from ref. 19; □, from ref. 20; ○, from ref. 21. The band of values obtained by Mehl *et al.* [18] is also shown.

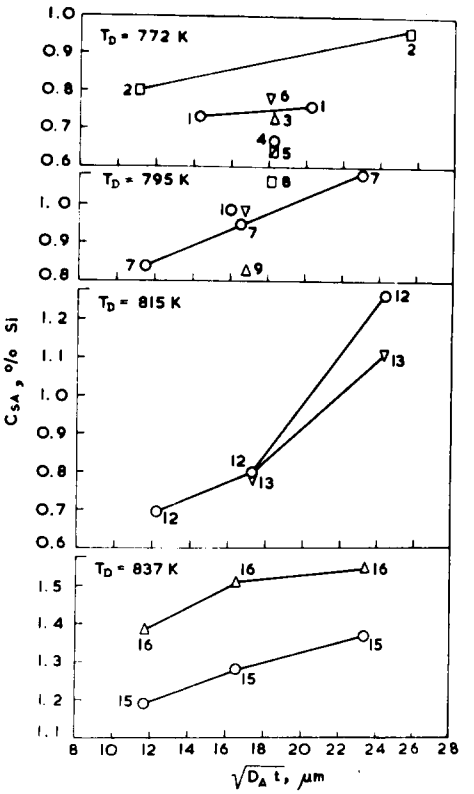

Fig. 5. C_{SA} *vs.* $(D_A t)^{1/2}$ at 772, 795, 815 and 837 K. The numbers at the data points indicate the precipitate.

The activation energy for dissolution of the silicon precipitates calculated from the slope of the Arrhenius plot in Fig. 3 amounts to 158 kJ mol^{-1}. In contrast, the activation energy for the diffusion of silicon in pure aluminium [11] lies between 120 and 160 kJ mol^{-1} with a most probable value of 127 kJ mol^{-1}. The marginal discrepancy between the present result and the data reported in the literature may be due to the fact that the present study deals with silicon diffusion in Al–Si alloy and not in pure aluminium. Silicon interacts strongly with vacancies in aluminium [25] and the solute–vacancy binding energy for silicon reported by Takamura [26] is equal to 25 ± 3 kJ mol^{-1}. In the alloy matrix under consideration the concentration of silicon atoms is sufficient to form solute–vacancy complexes with all the vacancies and thereby to increase the activation energy for the diffusion of silicon atoms freshly dissolving in the matrix.

3.3. Variation of the solute concentration at the interface

Figure 5 shows the variation of C_{SA} with $(D_A t)^{1/2}$ at four dissolution temperatures. It is interesting that C_{SA} for grain boundary allotriomorphs (*e.g.* precipitate 2) as well as for matrix precipitates (*e.g.* precipitate 12) does not remain constant but increases with time, *i.e.* that the silicon concentration in the matrix at the phase boundary does not attain steady state during the present solution treatment, indicating that the dissolution process is governed by an interface reaction. In addition, the figure shows that C_{SA} for a given value of $(D_A t)^{1/2}$ and/or temperature may be different for different particles.

At this point we may question the applicability of eqn. (1) with the initial condition

$$C = C_S \qquad \text{for } x = 0,\ t > 0 \tag{3}$$

For the alloy system under investigation, however, the exact rate equation for solute transfer at the interface is unknown. Moreover, the kinetics may not be the same for different precipitates, as suggested by the diversity of the slopes of the curves in Fig. 5. Nevertheless, the simplest assumption may be that

$$-D\frac{\partial C}{\partial x} = k(C_E - C_S) \qquad \text{for } x = 0 \tag{4}$$

where k is a constant of proportionality and C_E is the equilibrium solute concentration.

If the interface is stationary the concentration profile in a semi-infinite medium subjected to condition (4) can be defined by [23]

$$C = C_M + (C_E - C_M)\left[\operatorname{erfc}\left\{\frac{x}{2(Dt)^{1/2}}\right\} - \exp\left(\frac{kx + k^2 t}{D}\right)\operatorname{erfc}\left\{\frac{x}{2(Dt)^{1/2}} + k\left(\frac{t}{D}\right)^{1/2}\right\}\right] \quad (5)$$

Both the existing literature [27] and the present regression program show that diffusion data fitted to eqn. (5) yield C_S values almost identical with those obtained from eqn. (1). However, from the computational standpoint, eqn. (5) is quite difficult to treat. In any case the numerical values of the solute content at the interface reported in this paper seem to be sufficiently accurate.

3.4. *Effects of precipitate–matrix orientation*

No systematic difference between the solution kinetics of grain boundary allotriomorphs and of matrix precipitates was observed in the present investigation. However, Smith's classification of precipitate morphology [28] defines high energy and low energy interfaces of an allotriomorph. In order to compare the solute transfer characteristics across these two types of boundary, particles with $\theta = 0$, *i.e.* precipitates 1 and 14, were selected and the natures of their phase boundaries were identified. Estimates of C_S at the two types of boundary are presented in Table 2 for both precipitates.

The observations are rather limited and further detailed analysis in this direction is warranted to provide a more meaningful interpretation. However, it appears that in the early stage of solution treatment ($(D_A t)^{1/2} < 14.5\ \mu m$) C_S is marginally greater at the high energy interface than at the low energy phase boundary. As dissolution progresses this difference in solute concentration almost disappears. In contrast, C_{SA} is significantly different for different precipitates under similar dissolution conditions and the rate of change of C_{SA} is possibly different for different particles. The slow cooling rate employed in the present experiments during second-phase formation tends to promote precipitates with random orientation [13]. The difference in dissolution rates for different precipitates may therefore be attributed to the variation in structure of the phase boundaries.

TABLE 2

Solute concentrations at high energy and low energy interfaces

Preci-	T_D (K)	t (s)	$(D_A t)^{1/2}$ (μm)	C_S (% Si)	
				At high energy interface	*At low energy interface*
1	772	1500	14.3	0.76	0.69
				0.76	0.71
		3000	20.2	0.75	0.77
14	829	540	19.9	1.35	1.32

3.5. *The dissolution mechanism of silicon particles*

The nature of the present experiments precluded the possibility of contamination or SiO_2 layer formation at the precipitate–matrix interface and therefore the observed interface-reaction-controlled phenomenon cannot be attributed to these factors. We suggest that ledges are nucleated on the surfaces of dissolving precipitates and that silicon atoms from precipitates jump across the interface at the kinks in the ledges. It is proposed that nucleation of the ledges is the rate-limiting stage in the process of solution treatment. The frequency of nucleation of the ledges may not be identical at the different silicon–matrix interfaces, at least partly because of the heterogeneous structure of many dislocation boundaries [29], and this could be responsible for the observed divergence in the solute transfer characteristics of different precipitate particles.

4. CONCLUSIONS

During the early stage (*i.e.* $(D_A t)^{1/2} < 26$) of dissolution of silicon precipitates in Al–Si alloy the solute content of the aluminium-rich matrix at the phase boundary does not attain a steady state, indicating that the kinetics are being controlled by an interface reaction. The concentration of silicon at the interface increases gradually with solution treatment and the rate of increase may not be the same for different particles. There is possibly a differ-

ence in the solute transfer characteristics across different silicon–matrix interfaces. However, no systematic difference in the solution kinetics of grain boundary allotriomorphs and intragranular precipitates was observed.

The diffusivity values obtained for the dissolution of precipitates in the Al–Si alloy agree reasonably well with the existing data for the diffusion of silicon in pure aluminium. However, the activation energy of the former reaction seems to be slightly higher than the activation energy reported in the literature for the latter process.

ACKNOWLEDGMENTS

The author expresses his sincere appreciation of the help and inspiration received from Dr. O. N. Mohanty. Thanks are due to Alcan International Company, U. K., for the supply of superpure aluminium.

REFERENCES

1 P. A. Totta and R. P. Sopher, *IBM J. Res. Dev., 13* (1969) 226.
2 J. O. McCaldin and H. Sankur, *Appl. Phys. Lett., 19* (1971) 524.
3 J. O. McCaldin and H. Sankur, *Appl. Phys. Lett., 20* (1972) 171.
4 H. Sankur, J. O. McCaldin and J. Devaney, *Appl. Phys. Lett., 22* (1973) 64.
5 G. J. van Gurp, *J. Appl. Phys., 44* (1973) 2040.
6 J. S. Best and J. O. McCaldin, *J. Appl. Phys., 46* (1975) 4071.
7 L. D. Locker and C. D. Capio, *J. Appl.Phys., 44* (1973) 4366.
8 J. W. Mayer and K. N. Tu, *J. Vac. Sci. Technol., 11* (1974) 86.
9 H. Sankur and J. O. McCaldin, *J. Electrochem. Soc., 122* (1975) 565.
10 M. Hansen, *Constitution of Binary Alloys*, MacGraw-Hill, New York, 1958.
11 L. F. Mondolfo, *Aluminium Alloys: Structure and Properties*, Butterworths, London, 1976.
12 H. S. Rosenbaum and D. Turnbull, *Acta Metall., 6* (1958) 653.
13 H. S. Rosenbaum and D. Turnbull, *Acta Metall., 7* (1959) 664.
14 M. Hillert, *Metall. Trans., 6* (1975) 5.
15 J. W. Colby, personal communication, 1974.
16 C. S. Fuller and J. A. Ditzenberger, *J. Appl. Phys., 27* (1956) 544.
17 A. Beerwald, *Z. Elektrochem., 45* (1939) 789.
18 R. F. Mehl, F. N. Rhines and K. A. von den Steinen, *Met. Alloys, 13* (1941) 41.
19 H. Bückle, *Z. Elektrochem., 49* (1943) 238.
20 W. G. Fricke, Jr., *Trans. Am. Soc. Met., 58* (1965) 421.
21 D. Bergner and B. Cyrener, *Neue Hütte, 18* (1973) 356.
22 S. K. Pabi, *Acta Metall., 27* (1979) 1693.
23 J. Crank, *The Mathematics of Diffusion*, Oxford University Press, Oxford, 1956.
24 D. W. Marquardt, *J. Soc. Ind. Appl. Maths., 11* (1963) 431.
25 T. Federighi, Resistometric researches on point defects in quenched aluminium and aluminium-rich alloys. In R. M. Cottrill (ed.), *Lattice Defects in Quenched Metals*, Academic Press, New York, 1965, p. 217.
26 J. Takamura, Specimen size and quenched-in lattice defects. In R. M. Cottrill (ed.), *Lattice Defects in Quenched Metals*, Academic Press, New York, 1965, p. 521.
27 K. Abbott and C. W. Howorth, *Acta Metall., 21* (1973) 951.
28 C. S. Smith, *Trans. Am. Soc. Met., 45* (1953) 533.
29 H. I. Aaronson, C. Laird and K. R. Kinsman, Mechanisms of diffusional growth of precipitate crystals. In H. I. Aaronson (ed.), *Phase Transformations*, American Society for Metals, Metals Park, Ohio, 1970, p. 313.